Creating a low-symmetry insulating, ferroelectric, and antiferromagnetic material from a high-symmetrical metallic ferromagnet via defect engineering: The case of LaBaCo_{2}O_{5+δ} compounds

Yurong Yang, Chunrui Ma, Ming Liu, Hong Jian Zhao, Yuan Lin, Chonglin Chen, and L. Bellaiche

Phys. Rev. B **95**, 165132 — Published 24 April 2017

DOI: 10.1103/PhysRevB.95.165132

Creating a low-symmetrical insulating, ferroelectric, and antiferromagnetic material from a high-symmetrical, metallic ferromagnet via defect-engineering: the case of $LaBaCo_2O_{5+\delta}$ compounds

Yurong Yang[1*], Chunrui Ma[2,3,*], Ming Liu[4], Hongjian Zhao,[1,5], Yuan Lin,[6] Chonglin Chen[3] and L. Bellaiche[1]

1. Physics Department and Institute for Nanoscience and Engineering, University of Arkansas, AR 72701, USA
2. State Key Laboratory for Mechanical Behavior of Materials, Xi'an Jiaotong University, Shaanxi 710049, PRC
3. Department of Physics and Astronomy, University of Texas at San Antonio, TX 78249, USA
4. Electronic Materials Research Laboratory, Key Laboratory of the Ministry of Education and International Center for Dielectric Research, Xi'an Jiaotong University, Shaanxi, 710049, PRC
5. Laboratory of Dielectric Materials, Department of Materials Science and Engineering, Zhejiang University, Zhejiang, 310027, PRC
6. State Key Laboratory of Electronic Thin films and Integrated Devices, University of Electronic Science & Technology of China, Sichuan 610054, PRC

Abstract: First-principles calculations are performed to investigate properties of defect-free $LaBaCo_2O_6$ materials as well as $LaBaCo_2O_5$ films possessing ordered oxygen vacancy structures. These calculations predict that the defect-free $LaBaCo_2O_6$ crystallizes in a tetragonal state with an axial ratio smaller than unity, and is metallic and ferromagnetic as consistent with the literature. In contrast, the $LaBaCo_2O_5$ film adopt a low-symmetry monoclinic state having an axial ratio larger than 1, is insulating and even ferroelectric, as well as exhibit a G-type antiferromagnetic ordering. These calculations further reveal the origin of these defect-induced changes in properties. Moreover, experiments we further conducted demonstrate the possibility to grow highly-epitaxial $LaBaCo_2O_5$ films with ordered oxygen vacancies, via reduction treatments, and confirm some of our predictions. These findings can open a new avenue for the design and synthesis of multiferroics via defect-engineering.

PACS: 76.50.+g; 61.72.-y; 71.30.+h; 75.85.+t

[*] These authors contributed equally to this work.

I. Introduction

Cobalt oxides have been widely studied for many years due to their high chemical stability, excellent oxygen permeability, and many other unique physical chemistry properties for energy conversion, catalysts, sensors, and solid oxides fuel cells, etc. [1-4]. They also exhibit rich magnetic and electronic transport properties, ranging from paramagnetism to ferromagnetism via antiferromagnetism, from magnetic frustration to metal-insulator transition and colossal magnetoresistance, and many others [5-7]. These phenomena are highly dependent upon the degrees of freedom such as charge distribution, spin and orbital orderings, and lattice structures [8]. In addition, cobalt oxides can possess different cobalt and oxygen coordination from tetrahedral, pyramidal to octahedral depending on its oxygen content, which leads to various crystal structures having a great flexibility of the oxygen frameworks [9]. As a result, oxygen nonstoichiometry is a crucial parameter for tuning physical properties determined by their crystal structure [10]. Among the cobalt oxide family, $LaBaCo_2O_{5+\delta}$ (with $0 \leq \delta \leq 1$) (LBCO) exhibit anomalous physical properties such as giant magnetoresistance effect, superfast chemical dynamics, etc.[11-14]. Moreover, the achievement of fabricating (with various post-annealing treatments) an *ordered oxygen vacancy structure* in another related material, namely highly epitaxial $(La,Sr)CoO_{3-\delta}$ thin films, has opened up a new avenue for the studies of the ordered oxygen vacancy structures in Co-based systems [3, 15]. In particular, one may wonder if the formation of such structures with vacancies can dramatically alter properties of LBCO compounds, that are known to be metallic and ferromagnetic, within a tetragonal state having an axial ratio smaller than 1, when no or few oxygen vacancies exist in the materials [16, 17].

The goal of this Letter is to address this issue, by first performing and analyzing first-principles calculations. It is found that the creation of ordered oxygen vacancies inside LBCO

does result in original properties. Examples include the system becoming insulating, ferroelectric and antiferromagnetically-ordered, in addition to adopt a low-symmetry monoclinic phase having an axial ratio being larger than 1. Reasons behind such defect-induced changes are also unraveled. Finally, experiments are further conducted to demonstrate that the formation of ordered oxygen vacancies can occur inside high-epitaxial LBCO films and to confirm some of our striking predictions, which is promising for opening a route aimed at designing novel properties and multiferroics via defect-engineering.

II. Methods

In the present study, we perform first-principles calculations on two different types of LBCO supercell. The first type concerns the "defect-free" $LaBaCo_2O_6$ system, and is schematized in Fig. 1. Regarding the atomic arrangement of its A site atoms (La and Ba), it has pure La layers alternating, along the out-of-plane direction, with layers solely made of Ba. The second type of supercell is a $LaBaCo_2O_5$ structure and possesses (ordered) oxygen vacancies. Its supercell contains 10 O, 4 Co, 2 Ba and 2 La atoms, different A site atoms ordering are considered (see Fig. 2). The in-plane and out-of-plane lattice vectors and atomic positions are allowed to relax in order to minimize the total energy and obtain forces being smaller than 0.001 eV/Å on any ion**.** Practically, atomic relaxation and calculations of properties are carried out using density functional theory (DFT) within the framework of PBEsol+U [18, 19] and the projector augmented-wave potentials, as implemented in the VASP code [20]. The Hubbard U value for Co atoms is chosen to be U=2.5 eV. Note that we also tested values of U equal to 2, 3, 4, 5, 6, 7, and 8 eV within PBEsol+U, as well as the Heyd-Scuseria-Ernzerhof hybrid functionals [21]. All these different U values give the same antiferromagnetic ground state, lead to an

insulating character and very similar magnetic moment on Co atoms than those discussed and reported here (for PBEsol+U with U=2.5 eV) in the case of $LaBaCo_2O_6$. The energy cutoff is selected to be 550 eV, and the k-point mesh is taken to be $6 \times 6 \times 4$. The polarization is calculated by the Berry phase method [22]. Moreover, spin-orbit coupling and non-collinear magnetism are considered in order to investigate some magnetic properties of the defectuous LBCO.

III. Results

A. Properties of $LaBaCo_2O_6$

The defect-free LBCO (i.e., $LaBaCo_2O_6$) compound is predicted here to adopt a tetragonal symmetry with a *P4/mmm* space group (as a result of its layered structure), with an in-plane and out-of-plane lattice constants of 3.90 Å and 7.527 Å, respectively- which yields a normalized axial ratio of c/a=0.965, that is smaller than 1. Our *ab-initio* calculations also yield that this defect-free system is metallic and is a ferromagnet having a spontaneous total magnetization of 2.5 μ_B per five atoms, as consistent with Refs. [16, 17] [note that (i) we numerically checked the energies of the ferromagnetic and C-, G- and A-type antiferromagnetic orderings, and found the ferromagnetic (FM) structure to have the lowest energy in $LaBaCo_2O_6$; and (ii) the magnetization around each Co ions in the ferromagnetic state is found to be slightly smaller than 2.5 μ_B per five atoms, namely it is 2.2 μ_B, atoms because oxygen and other ions also contribute to the total magnetization].

B. Structure of $LaBaCo_2O_5$

Figure 2 depicts different presently considered structures all exhibiting ordering of La and Ba ions along the [001] direction. Configuration L1 is constructed from the bulk perovskite structure having the *I4cm* space group (which possesses $a^0a^0c^-$ oxygen octahedral tilting pattern and an electrical polarization along the [001] direction) by removing two O atoms in a (001) Co-O plane and then relaxing the resulting configuration. Configuration L2 is built the same way but by removing two nearest O atoms, and configuration L3 is built by removing one O atom in each (001) Co-O plane. Finally, Configurations $L4_{La}$ and $L4_{Ba}$ are constructed by removing O atoms in La-O and Ba-O planes, respectively (note that we also constructed similar configurations, but starting from cubic or R3c bulk perovskite, and obtain results that are similar to those starting from the I4cm space group of bulk perovskite). We also built structures we denote as RS1, RS2, RS3 and RS4 and that can be deduced from the L1, L2, L3 and L4 structures, respectively, by making the arrangements between La and Ba ions being of rocksalt-type. Table 1 reports the total energy of all these relaxed configurations, further considering four different types of magnetic ordering for each configuration: G-type antiferromagnetic (G-AFM), C-type antiferromagnetic (C-AFM), A-type antiferromagnetic (A-AFM) and ferromagnetic (FM).

We also built other configurations, still having a $LaBaCoO_5$ stoichiometry but adopting the Brownmillerite structure. These configurations are shown in Figure 3 and their energy is indicated in Table 2 for the different aforementioned magnetic orderings. BM-L1 possesses one La-O layer and one Ba-O layer that alternate along the [001] direction. On the other hand, in BM-L2 and BM-L3, two neighboring layers La-O alternate with two neighboring Ba-O layers along [001], and BM-RS exhibits a rocksalt ordering between La and Ba atoms. Tables 1 and 2 reveal that the three lowest-in-energy structures are L2, $L4_{La}$, and BM-L2, and that they each prefer a G-type antiferromagnetism. Their axial ratio is numerically found to be 1.017, 0.953, and 0.983. In other words, L2 is the only lowest-in-energy structure that adopts an axial ratio that

is larger than 1, which is precisely the type of axial ratio that our current measurements find (see the Supplemental Materials [23], where an experimental value of 1.023 is reported for the axial ratio). Moreover, L2 has the same type of oxygen vacancies arrangement (namely, occurring in planes containing Co ions) with the one experimentally found and reported in Figure 6. Therefore, we choose L2 structure for investigating the properties in $LaBaCo_2O_5$. Note that L2 can be considered to be a novel structure since we are not aware that it has ever been reported before, unlike L4 [24, 25] and the Brownmillerite structure [26, 27]. Note also that we numerically found (not shown here) that $L4_{La}$, and BM-L2 have strongly unstable phonons when epitaxially grown on $SrTiO_3$ (as done in the experiments described below), which further explains why we focused on L2 in the manuscript. Furthermore, the fact that Table 1 indicates that L2 has a higher computed energy than $L4_{La}$ implies that L2 is a metastable state, rather than the ground state, at low temperature. Such state can either become the ground state at finite temperature or is accessible by measurements even if it is not the ground state, which would explain its experimental observation (see the Supplemental Materials [23]).

C. Properties of $LaBaCo_2O_5$

The L2 structure of $LaBaCo_2O_5$ is found to have a monoclinic symmetry with a space group of *Pc*, and its computed in-plane lattice constants have a magnitude of 3.96 Å, while the out-of-plane lattice parameter is about 8.06 Å, which yields a normalized axial ratio of c/a=1.018 (and which is thus larger than 1). It is also found to be insulating and to possess a polarization having an out-of-plane component (i.e., along the pseudo-cubic [00-1] axis) of about 1.3 $\mu C/cm^2$ of magnitude**,** and an in-plane component of about 6.1 $\mu C/cm^2$ along the pseudo-cubic [110] direction. Note that the fact that this polarization has both in-plane and out-of-plane components

is consistent with the monoclinic symmetry of the ground state and that these components of the polarization can be altered by epitaxial strain. Moreover, the defectuous LBCO system presents a magnetic ordering that consists of a primary G-type antiferromagnetic vector lying along the [110] direction *and* a secondary ferromagnetic order being along the perpendicular [1-10] direction, yielding a magnetization of about $0.04\mu_B$ per Co atoms. Such latter weak magnetization originates from the spin-orbit-induced canting of the magnetic moment of the tetrahedral Co ions. In other words, playing with oxygen vacancies in LBCO can transform the system from a ferromagnetic metal of tetragonal symmetry to a predominantly antiferromagnetic and insulating material possessing an electrical polarization altogether with a weak magnetization, and adopting a low-symmetry monoclinic ground state. Defect-engineering in LBCO is therefore promising to alter and control various properties, and create new multiferroics.

Let us now concentrate on the out-of-plane component of the polarization of the L2 structure of $LaBaCo_2O_5$, that adopts a magnitude of about 1.3 $\mu C/cm^2$. To reveal its origin, Table 3 provides the polarization associated with the (001) La-O, Ba-O, Co-O_2 and Co-O layers and arising from the fact that the cation and oxygen atoms move away from each other in each of these four types of planes (i.e., these layers exhibit a rumpling). These polarizations are computed as the product between the effective charges of the ions and their displacement with respect to their ideal positions. Table 3 reveals that the overall out-of-plane polarization of the defectuous LBCO system is pointing down and arises from the incomplete compensation between the dipole moments (i) formed around the Ba-O layers and those formed near the La-O layers; and (ii) formed around the Co(T)-O layers (with Co being tetrahedral) and those formed near the Co(O)-O_2 layers (with Co being octahedral). Note that Item (ii) is reminiscent of a result

in $Sr_{1-x}Ba_xMnO_3$ [28] for which magnetic ions were found to contribute to polarization. Moreover, items (i) and (ii) can also be understood by simple electrostatics. For that, let us first assume that the Co ions being in an octahedral environment are charged +3 while those being in a tetrahedral environment are charged +2 to ensure that $LaBaCo_2O_5$ is neutral (note that this assumption is not only consistent with the built-in polarization we computed by Berry phase in $LaBaCo_2O_5$, but also with the charges exhibited by octahedral and tetrahedral Co ions in Co_3O_4 material [18, 29]). As a result, the modeled defectuous LBCO film presents two different types of CoO planes: one is $Co^{+2}O^{-2}$ that is neutral, and the other one is $Co^{+3}O_2^{-2}$ that is charged -1. The electric dipoles centered in the LaO planes being in-between $Co^{+2}O^{-2}$ and $Co^{+3}O_2^{-2}$ planes therefore experience an internal electric field being down (i.e., oriented towards the $Co^{+3}O_2^{-2}$ planes), while the electric dipoles centered in the BaO planes being in-between $Co^{+2}O^{-2}$ and $Co^{+3}O_2^{-2}$ planes feel an internal electric field being up (i.e., oriented towards the $Co^{+3}O_2^{-2}$ planes). As evidenced by our DFT calculations reported in Table 1, LaO-centered (respectively, BaO-centered) dipoles are therefore created antiparallel (respectively, parallel) to the growth direction because of these internal fields. Similarly, since BaO planes are neutral while LaO planes are charged +1, Co(T)O-centered (respectively, $Co(O)O_2$-centered) dipoles are aligned along (respectively, opposite to) the growth direction because of internal fields. This electrostatically-driven formation of the out-of-plane polarization also provides an explanation for another of our prediction that has not been discussed yet, namely why we did not find any stable state for which this out-of-plane component is reverted, that is, it points up rather than down.

We also numerically found that the ground state of the defectuous LBCO compound is doubly degenerate, with the resulting two states having the same out-of-plane polarization while having *opposite* in-plane polarizations. To understand its occurrence, Figure 4 shows a top view of the atomic structure of the two degenerate ground states. Let us first indicate again that

defectuous $LaBaCo_2O_5$ system possesses two different types of Co ions: Co ions that are denoted as Co(O) and experiencing an octahedral environment due to their six neighboring oxygen atoms, leading to in-plane and out-of-plane Co-O bonds being 1.98 Å and 2.38 Å, respectively; Co ions that are coined Co(T) and that are tetrahedrally coordinated (they are located at the center of a CoO_4 tetrahedron), with resulting Co-O bonds being mainly parallel to the in-plane and out-of-plane directions of 1.92 Å and 1.80 Å, respectively. In Fig. 4, oxygen atoms belonging to the $Co(O)O_2$ planes are represented in gray while those in the Co(T)O planes are drawn in orange. One can clearly see that, the oxygen ions belonging to the Co(T)O planes (which are also the planes possessing oxygen vacancies) do not have the same in-plane atomic coordinates than the oxygen ions of the $Co(O)O_2$ planes. Such motions can be thought as causing the CoO_4 tetrahedra to rotate about the [001] direction in clockwise or anticlockwise fashion, and result in the existence of an in-plane polarization, P_{in}. Interestingly, P_{in} is along the pseudo-cubic [110] direction *versus* the pseudo-cubic [-1-10] direction in the left and right panels of Fig. 4, respectively, because the rotation about the [001] direction of the CoO_4 tetrahedra is reversed between these left and right panels. The configurations in these two panels have therefore the same energy and the same space group but opposite in-plane polarizations. Interestingly, the energy barrier between these two states is calculated to be 66 meV per CoO_4 tetrahedra, which is similar to the barrier energy of 76 meV per 5 atoms between the two states of opposite polarization in the ferroelectric prototype $PbTiO_3$ [30]. Therefore, applying an electric field to defectuous LBCO should result in the reversal of this in-plane polarization via the switching between these two configurations, which makes such system ferroelectric.

D. Understanding the differences in properties between $LaBaCo_2O_6$ and $LaBaCo_2O_5$

Let us now try to better understand our predictions about the difference in electronic properties (metal *versus* insulator) and in magnetic orderings (ferromagnetic *versus* G-type antiferromagnetic) between the defect-free $LaBaCo_2O_6$ and the defectuous $LaBaCo_2O_5$ systems. For that, their computed electronic density of states are shown in Figs. 5(a)-(d). Note that spin-orbit interactions are not included in these computations. Figure 5a clearly demonstrates that the FM defect-free $LaBaCo_2O_6$ material is indeed predicted to be metallic since its Fermi energy (chosen as the zero in energy) falls in within bands. Its highest occupied valence states are made of O 2p electrons and Co 3d electrons. Figure 5a further indicates that the Co 3d t_{2g} orbitals heavily contribute (along with a small amount of O 2p electrons, not shown here) to the states located between -1 eV and ~1 eV, including the Fermi level. As a result, the Co 3d electrons of $LaBaCo_2O_6$ near the Fermi level are rather delocalized in the real space.

Regarding the G-type AFM $LaBaCo_2O_5$ system, Co(O) is numerically found to have a magnetic moment of ~2.5 μ_B, while Co(T) possesses a magnetic moment of ~2.8 μ_B. The G-type AFM $LaBaCo_2O_5$ compound is calculated to be an insulator with a small band gap of the order of 0.56 eV, as evidenced in Fig. 5b. Like in defect-free $LaBaCo_2O_6$, (i) the highest occupied states are made of O 2p electrons (not shown here) mixed with Co 3d t_{2g} orbitals (see Fig. 5d); (ii) the lowest unoccupied conduction states (in the energy range of ~0.56 eV to ~3 eV above the Fermi energy) are mostly made of Co 3d orbitals being mixed with a few percentage of O 2p electrons. Figures 5c and 5d also reveal that the occupied states being near the valence band maximum involve the t_{2g} states of the "octahedral" Co(O) ion while the unoccupied states located close to the conduction band minimum are rather made of the t_2 orbitals of the tetrahedra Co(T) ion, which therefore explains why, unlike the defect-free $LaBaCo_2O_6$ compound (that has only one type of Co ion), $LaBaCo_2O_5$ is insulator and possesses localized Co 3d electrons.

Let us now try to understand the origin for the difference in magnetic ordering between $LaBaCo_2O_6$ and $LaBaCo_2O_5$, by using a simple model. For that, Figs. 5e and 3f show the schematic description of the Co 3d energy level of these two oxides, respectively. The crystal field (octahedral environment) splits the 3d orbitals of the Co ions in $LaBaCo_2O_6$ in the manner shown in Fig. 5e. Here, each Co ion has a nominal ionic charge of +3.5 in order to make the whole system neutral. As a result, every Co ion has five 3d electrons that can be arranged in the spin configuration shown in Fig. 5e *and* there is an additional electron that is shared by two neighboring Co ions in $LaBaCo_2O_6$. Such additional electron is the so-called itinerant electron, and can thus transfer back and forth from one Co ion to the other one (as schematized by the green dashed dot curve line of Fig. 5e). In the schematization of Fig. 5e, $LaBaCo_2O_6$ is therefore metallic and ferromagnetic, as computationally found. According to this picture, each Co ion should have an averaged magnetic moment of 5/2=2.5 μ_B, which is rather consistent with the first-principle value of 2.2 μ_B.

On the other hand, the two different types of crystal field existing in $LaBaCo_2O_5$ (because of octahedral *versus* tetrahedral environment) split the 3d orbitals of Co ions in the manner shown in Fig. 5f: the t_{2g} orbitals have lower energy than the e_g orbitals in the Co(O) sites, while the reverse situation applies to the Co(T) sites. In addition and as indicated above, the Co(O) and Co(T) ions are expected to have a nominal charge of +3 and +2, respectively, which leads to each Co(O) ion having six 3d electrons while there are seven 3d electrons surrounding each Co(T) ion. Figure 5f shows the proposed simple model of the electron configurations for Co(O) and Co(T) and the corresponding exchange interactions. The e_g and t_{2g} orbitals in Co(O) and half-filled t_2 orbitals in Co(T) lead to three kinds of interactions, Co(O)-Co(T), as well as Co(O)-Co(O) and Co(T)-Co(T) interactions. As is shown in Fig. 5f, for Co(O)-Co(T), there are super-exchange interactions between Co(O)'s e_g and Co(T)'s t_2, as well as between Co(O)'s t_{2g} and

Co(T)'s t_2. For Co(O)-Co(O), there are e_g - e_g, t_{2g}- t_{2g}, and t_{2g}- e_g super-exchange interactions. Finally, for Co(T)-Co(T), there is only the t_2- t_2 super-exchange interaction. As a result and according to the Goodenough-Kanamori rule [31, 32], all these super-exchange interactions are antiferromagnetic in nature, and thus leads to an overall G-type AFM ordering. This occupation of orbitals lead to 3 μ_B for Co(T) and 4μ_B for Co(O). Our DFT calculations does confirm this value close to 3 μ_B for Co(T) (it is ~2.8 μ_B), but provides a smaller than expected value for the magnetization of Co(O) (it is numerically found to be ~2.5μ_B rather than 4 μ_B). Such latter discrepancy arises from the fact that the 3d orbitals of Co(O) hybridize with the oxygen orbitals and that such hybridization is not included in the model associated with Fig. 5f. Note that such hybridization also explains why the magnetic moment of Fe ions in $BiFeO_3$ is found to be close to 4μ_B by experiments [33] and first-principles calculations [34], while an energetic diagram similar to Figs. 5e and 5f and only involving 3d orbitals, yields a higher value of 5 μ_B.

We also conducted experiments, mostly to demonstrate that defect-engineering can indeed been conceived in LBCO (but also to help us determine which structure to theoretically investigate). We also expose as-grown LBCO thin film grown on a Nb-doped $SrTiO_3$ (Nb:STO) substrate under oxygen annealing treatments but also under vacuum post annealing treatments. Annular bright field (ABF) scanning transmission electron microscopy (STEM) imaging techniques were performed in cross-section samples. As shown in Fig. 6 and discussed in the Supplementary Materials [23], the ABF image is consistent with the existence of the (novel) defectuous $LaBaCo_2O_5$ structure with ordered oxygen vacancies we computationally investigated. As further indicated in the Supplemental Materials [23], measurements also confirm our predictions that defectuous $LaBaCo_2O_5$ has a weak magnetization of the order of 0.02-0.04μ_B per f.u. and an axial ratio close to 1.02, while defect-free $LaBaCo_2O_6$ is ferromagnetic with an axial ratio smaller than 1.

IV. Conclusions

Our first-principle calculations were employed to reveal the possibility of transforming LBCO systems from ferromagnetic and metallic to antiferromagnetic, insulator and ferroelectric, via the creation of ordered oxygen vacancies. Analysis of the results also explains the reasons behind such striking transformations. Finally, growths and measurements were conducted to demonstrate that defect-engineering is practical in these systems and to confirm some of our predictions, which is therefore a promising route to design materials with novel properties and new multiferroics.

Y.Y. and L.B. acknowledge ONR Grant N00014-12-1-1034. This research was also partially supported by the Department of Energy under DE-FE0003780, and the Natural Science Foundation of China under 11329402 and 51202185. Also, C. M would like to acknowledge the support from the "China Scholarship Council" for the program of national study-abroad project for the postgraduates of high-level universities at UTSA.

References

[1] X. Xie, Y. Li, Z.-Q. Liu, M. Haruta, and W. Shen, Nature **458**, 746 (2009).

[2] G. Kim, S. Wang, A. J. Jacobson, Z. Yuan, W. Donner, C. L. Chen, L. Reimus, P. Brodersen, and C. A. Mims, Appl. Phys. Lett. **88**, 024103 (2006).

[3] Y. M. Kim, J. He, M. D. Biegalski, H. Ambaye, V. Lauter, H. M. Christen, S. T. Pantelides, S. J. Pennycook, S. V. Kalinin, and A. Y. Borisevich, Nat. Mater. **11**, 888 (2012).

[4] J. Liu, M. Liu, G. Collins, C. L. Chen, X. N. Jiang, W. Q. Gong, A. J. Jacobson, J. He, J. C. Jiang, and E. I. Meletis, Chem. Mater. **22**, 799 (2010).

[5] V. G. Bhide, D. S. Rajoria, C. N. R. Rao, G. R. Rao, and V. G. Jadhao, Phys. Rev. B **12**, 2832 (1975).

[6] F. Fauth, E. Suard, V. Caignaert, B. Domenges, I. Mirebeau, and L. Keller, EPJ B **21**, 163 (2001).

[7] J. B. goodenough, J. Phys. Chem. Solids **6**, 287 (1958).

[8] A. Maignan, C. Martin, D. Pelloquin, N. Nguyen, and B. Raveau, J. Solid State Chem. **142**, 247 (1999).

[9] B. Raveau, Phil. Trans. R. Soc. A **366**, 83 (2008).

[10] M. M. Seikh, C. Simon, V. Caignaert, V. Pralong, M. B. Lepetit, S. Boudin, and B. Raveau, Chem. Mater. **20**, 231 (2008).

[11] M. Liu, J. Liu, G. Collins, C. R. Ma, C. L. Chen, J. He, J. C. Jiang, E. I. Meletis, A. J. Jacobson, and Q. Y. Zhang, Appl. Phys. Lett. **96**, 132106 (2010).

[12] M. Liu, C. R. Ma, J. Liu, G. Collins, C. L. Chen, J. He, J. C. Jiang, E. I. Meletis, L. Sun, A. J. Jacobson, et al., ACS Appl. Mater. Interfaces **4**, 5524 (2012).

[13] C. R. Ma, M. Liu, G. Collins, J. Liu, Y. M. Zhang, C. L. Chen, J. He, J. C. Jiang, and E. I. Meletis, Appl. Phys. Lett. **101**, 021602 (2012).

[14] C. R. Ma, M. Liu, G. Collins, H. B. Wang, S. Y. Bao, X. Xu, E. Enriquez, C. L. Chen, Y. Lin, and M. H. Whangbo, ACS Appl. Mater. Interfaces **5**, 451 (2013).

[15] W. Donner, C. L. Chen, M. Liu, A. J. Jacobson, Y. L. Lee, M. Gadre, and D. Morgan, Chem. Mater. **23**, 984 (2011).

[16] E.-L. Rautama, P. Boullay, A. K. Kundu, V. Caignaert, V. Pralong, M. Karppinen, and B. Raveau, Chem. Mater. **20**, 2742 (2008).

[17] T. Nakajima, M. Ichihara, and Y. Ueda, J. Phys. Soc. Jpn. **74**, 1572 (2005).

[18] L. Chen, Y. R. Yang, and X. K. Meng, Appl. Phys. Lett. **102**, 203102 (2013).

[19] J. P. Perdew, A. Ruzsinszky, G. I. Csonka, O. A. Vydrov, G. E. Scuseria, L. A. Constantin, X. L. Zhou, and K. Burke, Phys. Rev. Lett. **100**, 136406 (2008).

[20] G. Kresse and D. Joubert, Phys. Rev. B **59**, 1758 (1999).
[21] J. Heyd, G. E. Scuseria, and M. Ernzerhof, J. Chem. Phys. **124**, 219906 (2006).
[22] R. D. King-Smith and D. Vanderbilt, Phys. Rev. B **47**, 1651 (1993).
[23] See Supplemental Material at [URL].
[24] W. Donner, C. Chen, M. Liu, A. J. Jacobson, Y.-L. Lee, M. Gadre, and D. Morgan, Chem. Mater. **23**, 984 (2011).
[25] S. Sengodan, S. Choi, A. Jun, T. H. Shin, Y.-W. Ju, H. Y. Jeong, J. Shin, J. T. S. Irvine, and G. Kim, Nat. Mater. **14**, 205 (2015).
[26] Y.-M. Kim, J. He, M. D. Biegalski, H. Ambaye, V. Lauter, H. M. Christen, S. T. Pantelides, S. J. Pennycook, S. V. Kalinin, and A. Y. Borisevich, Nat. Mater. **11**, 888 (2012).
[27] Y. Ito, R. F. Klie, N. D. Browning, and T. J. Mazanec, J. Am. Ceram. Soc. **85**, 969 (2002).
[28] H. Sakai, J. Fujioka, T. Fukuda, D. Okuyama, D. Hashizume, F. Kagawa, H. Nakao, Y. Murakami, T. Arima, A. Q. R. Baron, et al., Phys. Rev. Lett. **107**, 137601 (2011).
[29] J. Chen, X. Wu, and A. Selloni, Phys. Rev. B **83**, 245204 (2011).
[30] S. P. Beckman, X. Wang, K. M. Rabe, and D. Vanderbilt, Phys. Rev. B **79**, 144124 (2009).
[31] J. B. Goodenough, Phys. Rev. **100**, 564 (1955).
[32] J. Kanamori, J. Phys. Chem. Solids **10**, 87 (1959).
[33] P. Fischer, M. Polomska, I. Sosnowska, and M. Szymanski, J. Phys. C **13**, 1931 (1980).
[34] J. B. Neaton, C. Ederer, U. V. Waghmare, N. A. Spaldin, and K. M. Rabe, Phys. Rev. B **71**, 014113 (2005).

Table 1. Energies of different considered atomic structures (deduced from the perovskite structure) with different magnetic configurations (in eV/f.u.). The zero of energy is chosen to correspond to the L2 structure adopting a G-type antiferromagnetism.

	G-AFM	C-AFM	A-AFM	FM
L1	0.462	0.434	0.414	0.255
L2	0.000	0.157	0.086	0.197
L3	0.422	0.102	0.409	0.362
$L4_{La}$	-0.110	-0.003	0.078	0.199
$L4_{Ba}$	1.094	1.335	0.937	1.433
RS1	0.785	0.894	0.571	0.536
RS2	0.043	0.163	0.111	0.218
RS3	0.755	0.898	0.809	0.838
RS4	0.900	0.966	1.089	1.178

Table 2. Energies of different Brownmillerite structures with different magnetic configurations (in eV/f.u.). The zero of energy is chosen to correspond to the L2 structure adopting a G-type antiferromagnetism.

	G-AFM	C-AFM	A-AFM	FM
BM-L1	0.035	0.058	0.153	0.247
BM-L2	0.005	0.096	0.104	0.301
BM-L3	0.132	0.264	0.271	0.354
BM-RS	0.130	0.230	0.068	0.161

Table 3. Born effective charges, cation-oxygen rumpling and corresponding contribution of the out-of-plane component of the polarization for the different (001) layers in the L2 structure of $LaBaCo_2O_5$.

Layer	La-O	Ba-O	Co(T)-O	Co(O)-O_2
Z_o (e)	4.26 (La) and -2.92 (O)	3.14 (Ba) and -3.18 (O)	3.75 (Co) and -1.97s8 (O)	1.33 (Co) and (-2.30,-2.09) for O
δ_o (Å)	-0.687	0.512	0.184	-0.165
P_o (μC/cm^2)	-20.9	20.1	9.5	-10.0

Figure Captions

Figure 1. (color online) Atomic structures used to mimic $LaBaCo_2O_6$ with no defect. The red, blue, green and light blue spheres represent O, Co, La and Ba ions, respectively.

Figure 2. (color online) Chosen configurations for $LaBaCo_2O_5$ compounds having A-site ordering along [001] and deduced from a perovskite structure. These configurations contain 18 atom per unit cell, and have lattice vectors ***a*** being along the [1-10] pseudo-cubic direction, ***b*** being oriented along the pseudo-cubic [110] direction, and ***c*** being along the pseudo-cubic [001] direction. The red, blue, green and light blue spheres represent O, Co, La and Ba ions, respectively.

Figure 3. (color online) Chosen Brownmillerite configurations for $LaBaCo_2O_5$ compounds having A-site ordering along [001] (Panels a-c) and being of rocksalt-type (Panel d). The red, blue, green and light blue spheres represent O, Co, La and Ba ions, respectively.

Figure 4. (color online) Top view of the atomic structures of the two degenerate ground states of $LaBaCo_2O_5$. The left panel and right panel configurations possess in-plane polarization, P_{in}, along the pseudo-cubic [110] direction and [-1-10] direction, respectively. The oxygen atoms in the $Co(O)O_2$ plane (Co in an octahedral environment) are shown in gray, while those belonging to the Co(T)O plane (Co in a tetrahedral environment) are depicted in orange. The other oxygen atoms are shown in red, while blue spheres correspond to Co ions. The light blue and green spheres represent Ba and La ions, respectively.

Figure 5. (color online) Computed electronic density of states and resulting proposed simple model. Panels (a) shows the total density of states of $LaBaCo_2O_6$ as well as *e* and t_2 states of Co ions in $LaBaCo_2O_6$. Panels (b) shows the total density of states of $LaBaCo_2O_5$. Panels (c) and (d) report *e* and t_2 orbitals density of states of the Co(T) and Co(O) in $LaBaCo_2O_5$, respectively. In Panels (a)-(d), the zero energy is set at the Fermi level, and positive and negative values of these density of states correspond to spin-up and spin-down channels, respectively. Panels (e) and (f) depict the schematic description for the energy levels of the Co 3d orbitals in $LaBaCo_2O_6$ and $LaBaCo_2O_5$ oxides, respectively. The solid blue and red solid arrows are for the *e* and t_2 electrons. In Panel (e), the red dashed arrow corresponds to the itinerant electron of $LaBaCo_2O_6$, and the green curved line symbolizes the transfer of the itinerant electron. Distorted CoO_6 octahedral and CoO_4 tetragonal entities both exist in $LaBaCo_2O_5$, therefore leading to Co ions

having either a +3 or a +2 nominal charge, as indicated in Panel (f). The different super-exchange interactions are represented by dashed lines in Panel (f).

Figure 6 (color online) ABF image of vacuum annealed LBCO thin film.

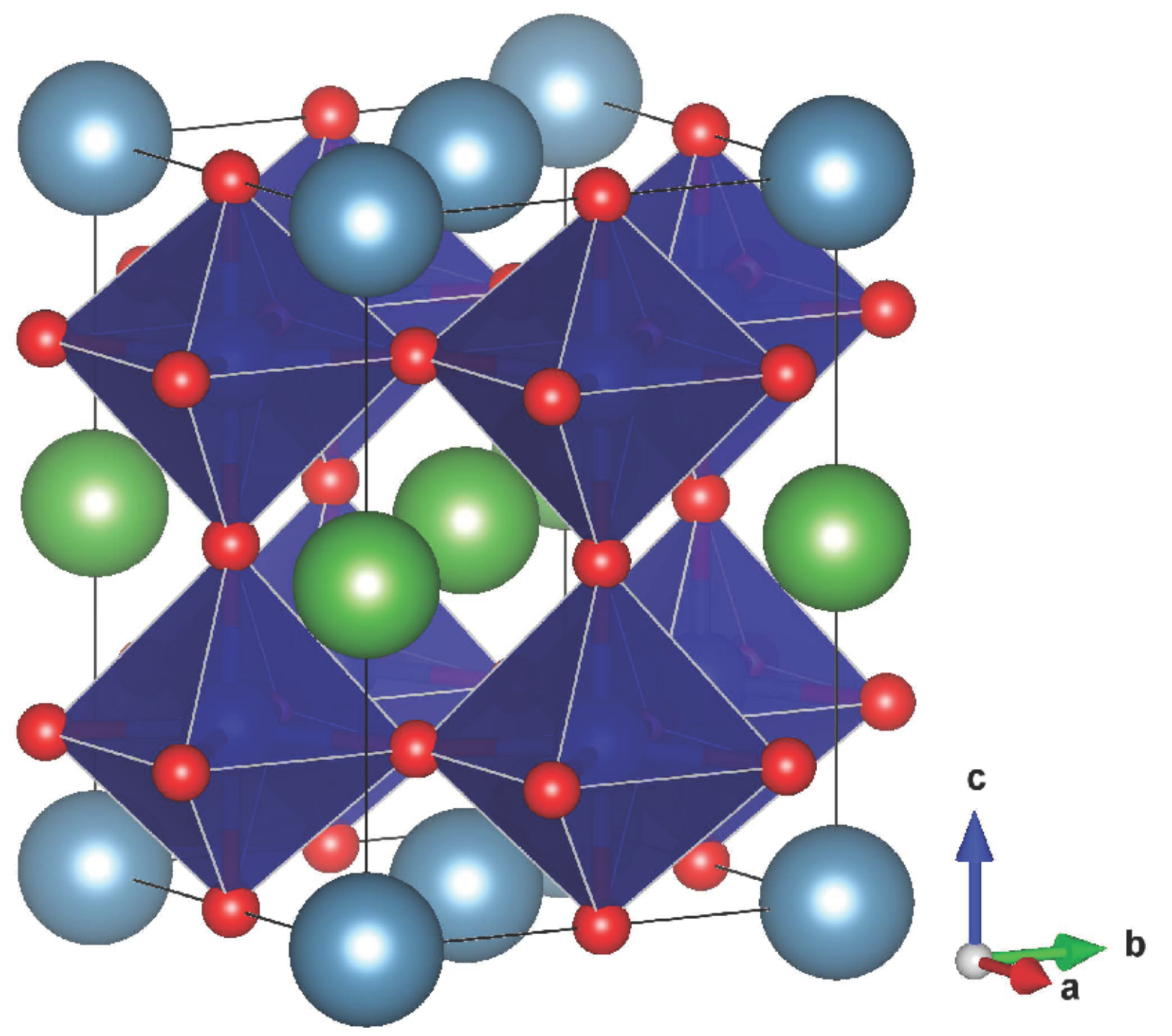
c
b
a

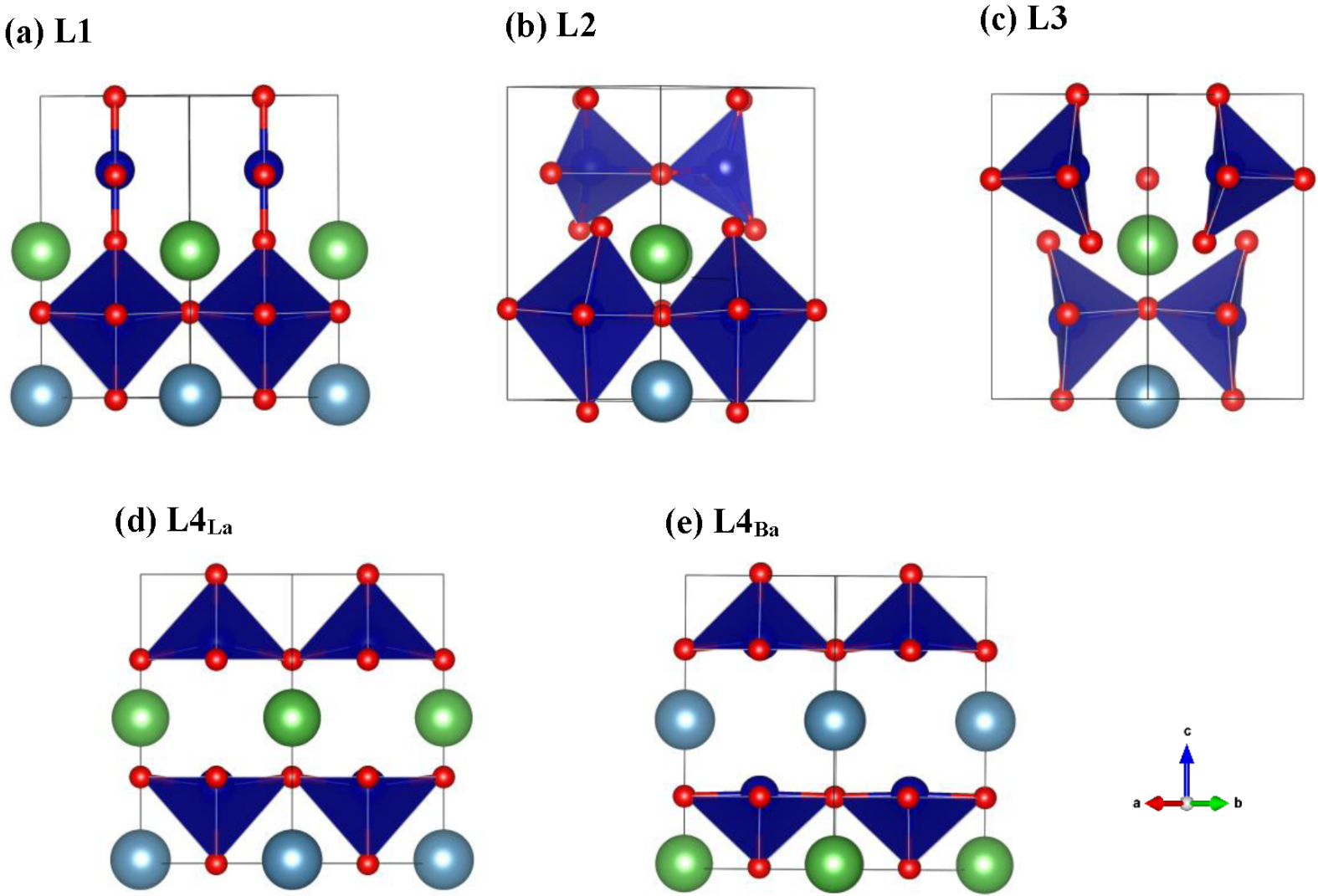
(a) L1
(b) L2
(c) L3
(d) L4La
(e) L4Ba
c
a
b

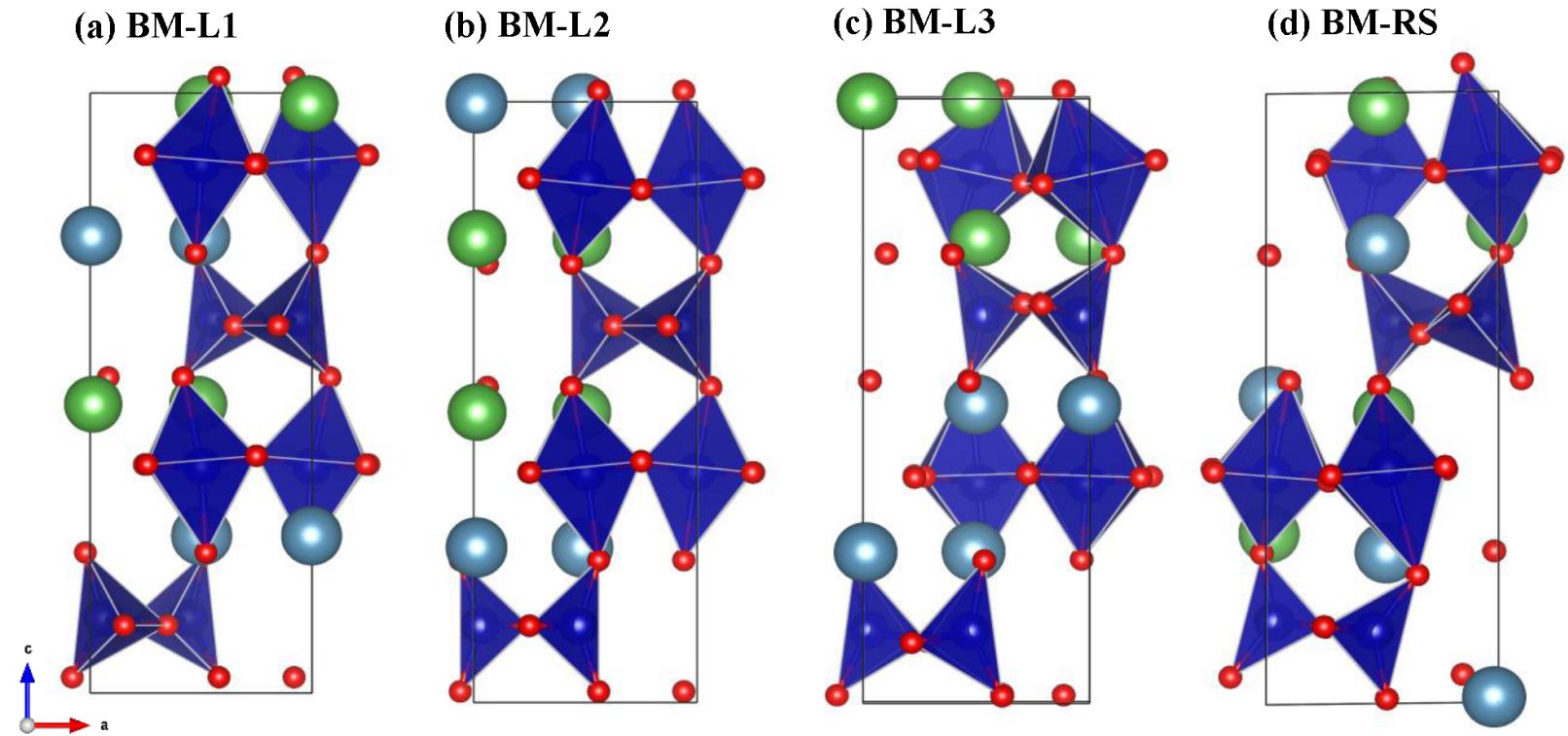
(a) BM-L1
(b) BM-L2
(c) BM-L3
(d) BM-RS
c
a

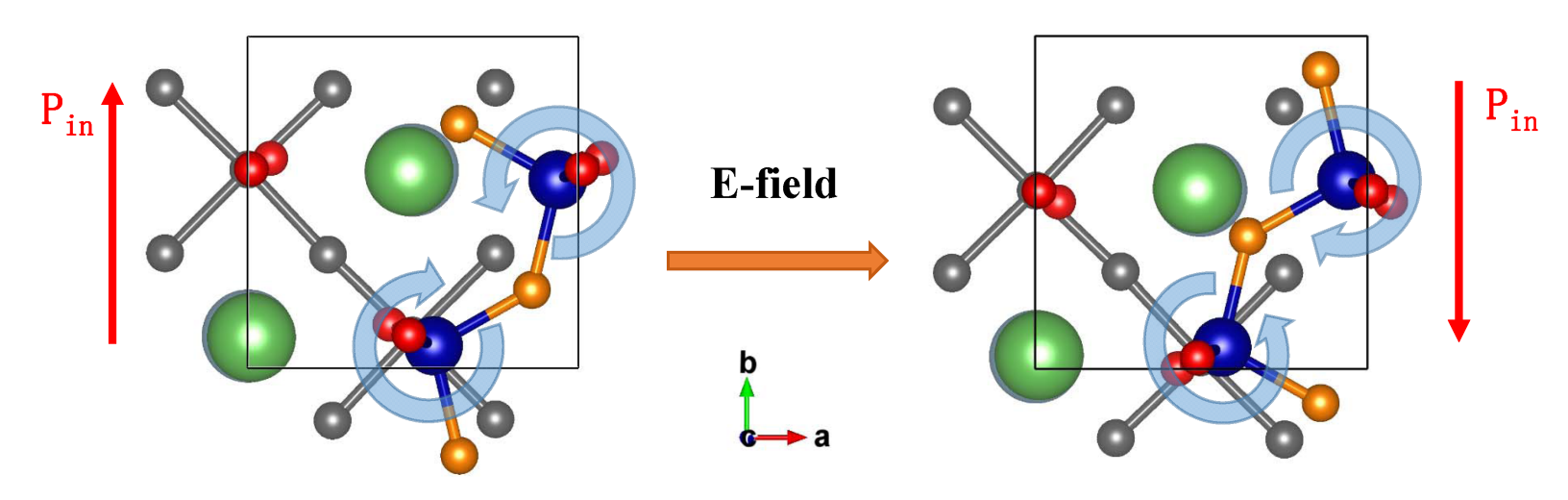
P in
E-field
b
c
a
P in

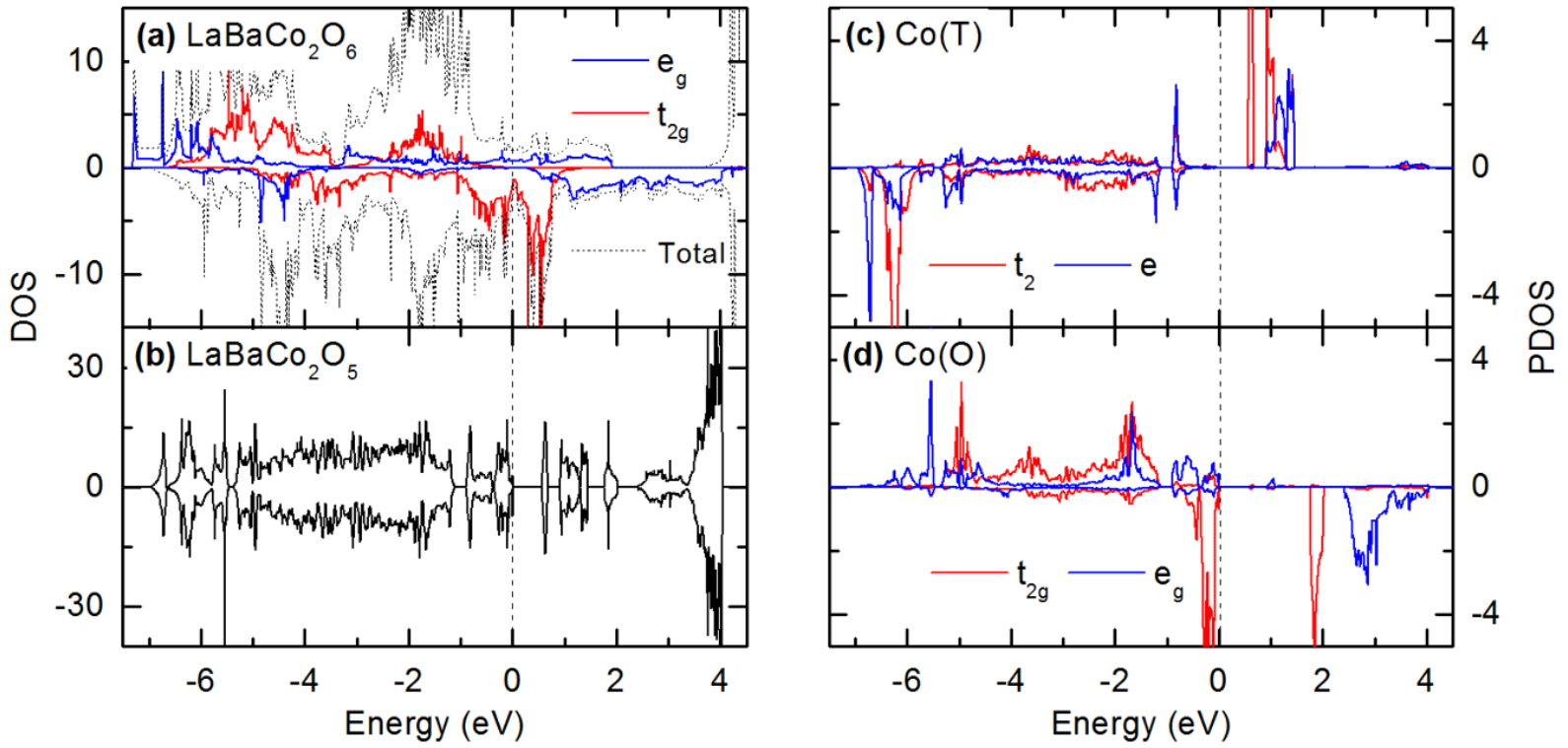
(a) LaBaCo2O6
eg
t2g
Total
(b) LaBaCo2O5
DOS
(c) Co(T)
t2
e
(d) Co(O)
t2g
eg
PDOS
Energy (eV)
Energy (eV)

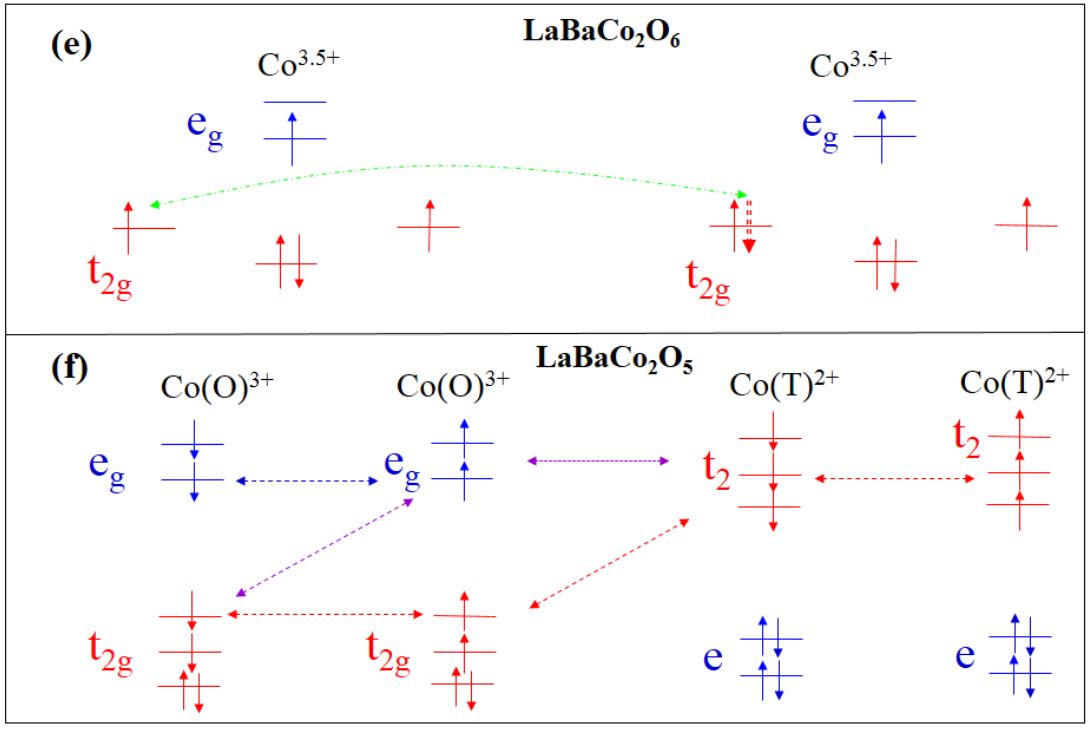
(e)
LaBaCo2O6
Co3.5+
Co3.5+
eg
eg
t2g
t2g
(f)
LaBaCo2O5
Co(O)3+
Co(O)3+
Co(T)2+
Co(T)2+
eg
eg
t2
t2
t2g
t2g
e
e

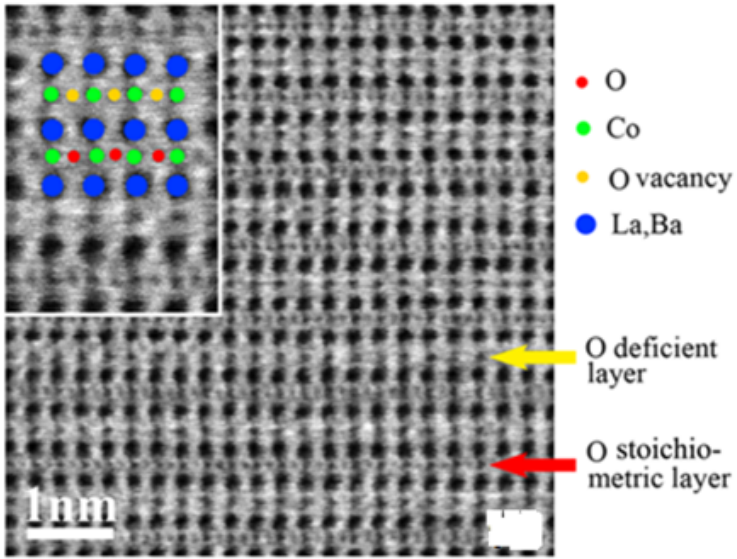
O
Co
O vacancy
La,Ba
O deficient layer
O stoichio-metric layer
1nm